



# Numerical modeling of optical coherent transient processes with complex configurations—II. Angled beams with arbitrary phase modulations

Tiejun Chang<sup>a,\*</sup>, Mingzhen Tian<sup>b</sup>, Zeb W. Barber<sup>b</sup>, Wm. Randall Babbitt<sup>a,b</sup>

<sup>a</sup>*The Spectrum Laboratory Montana State University, Bozeman, MT 59717, USA*

<sup>b</sup>*Physics Department, Montana State University, Bozeman, MT 59717, USA*

## Abstract

This work is a continuation of the development of the theoretical model for optical coherent transient (OCT) processes with complex configurations. A theoretical model for angled beams with arbitrary phase modulation has been developed based on the model presented in our previous work for the angled beam geometry. A numerical tool has been devised to simulate the OCT processes involving angled beams with the frequency detuning, chirped, and phase-modulated laser pulses. The simulations for pulse shaping and arbitrary waveform generation (AWG) using OCT processes have been performed. The theoretical analysis of programming and probe schemes for pulse shaper and AWG is also presented including the discussions on the rephasing condition and the phase compensation. The results from the analysis, the simulation, and the experiment show very good agreement.

© 2003 Elsevier B.V. All rights reserved.

*PACS:* 42.10; 42.10.M; 42.40

*Keywords:* Maxwell–Bloch equations; Optical coherent transient; Angled beam geometry; Frequency chirped pulse; Optical pulse shaper; Arbitrary waveform generator

## 1. Introduction

Optical coherent transient (OCT) techniques are not only well-established spectroscopic tools, but also the basis of a variety of proposed devices for optical information storage and processing [1–7]. To model the OCT processes, such as photon echoes, free induction decay and optical nutation, the coupled Maxwell–Bloch equations have been

used successfully for the collinear configuration in thick media [9–14]. In this theory the coherent effects of light on the inhomogeneously broadened absorbers are described by Bloch equations, where the electric field acts as a driving source to the atomic dipoles. The propagation effects are governed by Maxwell's equations, where the macroscopic polarization caused by the atomic dipole moments acts as a source to the electric field. Recently, more complex configurations have been proposed to make practical OCT-based devices, such as pulse shaper and arbitrary waveform generator [5–8]. This kind of devices requires

\*Corresponding author. Tel.: +1069947308;  
fax: +1469946767.

*E-mail address:* [chang@spectrum.montana.edu](mailto:chang@spectrum.montana.edu) (T. Chang).

angled beam configurations to discriminate the processed signals from unwanted transmitted inputs. In addition, the laser pulses are usually frequency detuned, chirped and phase and/or amplitude modulated. Frequency jitter and phase noise have to be taken into account in most practical settings as well.

In our previous work we developed a theoretical model based on Maxwell–Bloch equations for pulses with arbitrary phase modulations in collinear configuration and a model for multiple angled beam geometry without phase change [14]. However, neither of the two models can handle multi-beams combined with phase modulations. In this paper, we will develop a model to include both features by adding time-dependent phase terms to the model for multiple angled beam geometry. The numerical solution of the modified Maxwell–Bloch equation will be discussed for the development of the simulation tool. The OCT processes for pulse shaping and AWG will be discussed, in which the desired waveform is created as a photon echo sequence by a set of programming and probe pulses with complex features including frequency offset, linear chirp, and phase shift. The required rephasing condition and phase compensation will be derived analytically. Simulations using numerical tool will be presented for optical pulse shaping and AWG and compared with experimental results and the theoretical analysis.

## 2. Theoretical model angled beam with arbitrary phase modulations

In this section, we add a generalized phase term to the pulses in angled beam Maxwell–Bloch equations to develop a model for two beams, which is sufficient for simulations for pulse shapers and AWGs. The same treatment can be easily extended to multi-beams. We keep the two assumptions stated in Ref. [14], which are small angle and reflection free plane wave propagation in the medium. We define the vectors of the two angled beams as  $\vec{k}_- = \vec{k}_z - \vec{k}_x$  and  $\vec{k}_+ = \vec{k}_z + \vec{k}_x$ , respectively, where  $\vec{k}_z$  is the wave vector component in the general propagation direction and  $\vec{k}_x$  is

the component in the transverse direction  $x$ . Under the small angle assumption, we have  $\vec{k}_x \ll \vec{k}_z$  and  $|\vec{k}_z| \approx |\vec{k}|$ . We write the electric fields of the pulses propagating along the two beams as

$$E^\pm(x, z, t) = \frac{\hbar}{\mu} \Omega^\pm(x, z, t) \cos[\omega_0 t - k_z z \mp k_x x + \varphi^\pm(t)], \quad (1)$$

where  $+$  and  $-$  denote the two direction along  $\vec{k}_+$  and  $\vec{k}_-$ , respectively.  $\Omega^\pm$  represent the field amplitudes in the corresponding directions in term of Rabi frequency.  $\omega_0$  is an arbitrary stationary frequency usually chosen to be close to the atomic resonance.  $\varphi^\pm(t)$  are the time-dependent phases in the corresponding directions besides the spatial phase of the plane wave propagation and the phase from the field oscillation at the stationary frequency  $\omega_0$ . In general,  $\varphi^\pm(t)$  include all the effects of the frequency and phase modulations of the pulses, as well as the laser noises.

We can write the total electric field from both beams as

$$E(x, z, t) = \frac{\hbar}{\mu} [\Omega_C(x, z, t) \cos(\omega_0 t - k_z z) + \Omega_S(x, z, t) \sin(\omega_0 t - k_z z)] \quad (2)$$

with the in-phase and the in-quadrature components of the total field expressed as

$$\Omega_C(x, z, t) = \Omega^+(z, t) \cos[\varphi^+(t) + k_x x] + \Omega^-(z, t) \cos[\varphi^-(t) - k_x x], \quad (3)$$

$$\Omega_S(x, z, t) = -\Omega^+(z, t) \sin[\varphi^+(t) + k_x x] - \Omega^-(z, t) \sin[\varphi^-(t) - k_x x]. \quad (4)$$

The local interaction between the field and the atoms is described by Bloch equations as [14]

$$\frac{\partial r_1(x, z, t, \Delta)}{\partial t} = \Delta r_2(x, z, t, \Delta) + r_3(x, z, t, \Delta) \Omega_S(x, z, t) - \frac{r_1(x, z, t, \Delta)}{T_2}, \quad (5)$$

$$\frac{\partial r_2(x, z, t, \Delta)}{\partial t} = -\Delta r_1(x, z, t, \Delta) + r_3(x, z, t, \Delta) \Omega_C(x, z, t) - \frac{r_2(x, z, t, \Delta)}{T_2}, \quad (6)$$

$$\begin{aligned} \frac{\partial r_3(x, z, t, \Delta)}{\partial t} = & -r_2(x, z, t, \Delta)\Omega_C(x, z, t) \\ & -r_1(x, z, t, \Delta)\Omega_S(x, z, t) \\ & -\frac{1+r_3(x, z, t, \Delta)}{T_1}, \end{aligned} \quad (7)$$

where  $r_{1,2}$  are the in-phase and in-quadrature components of the atoms' polarization,  $r_3$ , the population inversion.  $T_2$  and  $T_1$  the coherent time and the lifetime of the excited state, respectively.  $\Delta = \omega_a - \omega_0$  denotes the detuning of the atoms' resonance  $\omega_a$  from the stationary frequency  $\omega_0$ .

The propagation of the field in the medium is governed by the Maxwell equations as

$$\frac{d\Omega_C(z, t)}{dz} = \frac{\alpha}{2\pi} \int_{-\infty}^{\infty} r_2(z, t, \Delta)g(\Delta) d\Delta, \quad (8)$$

$$\frac{d\Omega_S(z, t)}{dz} = -\frac{\alpha}{2\pi} \int_{-\infty}^{\infty} r_1(z, t, \Delta)g(\Delta) d\Delta, \quad (9)$$

where  $\alpha$  is the absorption coefficient of the medium and  $g(\Delta)$  represents the inhomogeneous spectral distribution of the atoms. The Maxwell–Bloch equation set has the same form as that in Ref. [14]. However, the rotating frames, in which the equations are valid, are completely different because of the different definitions of the rotating frequencies.

Due to the extra phase terms the formulas of the spatial Fourier transform become

$$\begin{aligned} \Omega^\pm(z, t) \cos[\varphi^\pm(t)] \\ = \frac{1}{2\pi} \int_0^{2\pi} [\Omega_C(x, z, t) \cos(k_x x) \\ \mp \Omega_S(x, z, t) \sin(k_x x)] d(k_x x), \end{aligned} \quad (10)$$

$$\begin{aligned} \Omega^\pm(z, t) \sin[\varphi^\pm(t)] \\ = \frac{1}{2\pi} \int_0^{2\pi} [\pm \Omega_C(x, z, t) \sin(k_x x) \\ + \Omega_S(x, z, t) \cos(k_x x)] d(k_x x). \end{aligned} \quad (11)$$

From these equations we can separate the field amplitude and phase of the pulses on each beam from the total field. The field of the pulses can also be calculated in term of the in-phase and in-quadrature components in the cases where small amplitude results in larger phase error.

The time-dependent phase terms introduced in this model enable us to simulate the OCT

processes involving the pulses with frequency and phase modulations in general. The only limit to the phase terms is to meet the slowly varying approximation [11]. The Maxwell–Bloch equations for angled beam with arbitrary phase modulation are solved numerically in the similar way as Ref. [14]. The discussions on the spatial, the temporal, and the spectral grid settings, Bloch vector initialization, propagation in thick medium, are also applicable in this model except the consideration of the time resolution in this case should take into account not only the time variation of the amplitude,  $\Omega^\pm(z, t)$  but also the phase,  $\varphi^\pm(t)$ .

### 3. Pulse shaping and AWG

The stimulated photon echo process has been proposed to perform pulse shaping and arbitrary waveform generation on a 1–100 GHz bandwidth [5]. This technique utilizes the optical processing ability of well-studied rare-earth-doped crystals, low-power linear-frequency chirped laser sources, and low bandwidth electronics to create desired high-band waveforms up to  $\sim 100$  GHz. Two schemes of programming and probing OCTs to perform pulse shaping and AWG are plotted in Fig. 1. In Fig. 1(a) the medium is programmed with a set of linear-frequency chirped square pulses consisting of a reference chirp and many control chirps of the same chirp rate,  $\beta$ . The reference propagates along direction  $\vec{k}_+$  and the control chirps along  $\vec{k}_-$ . The chirps start at different frequencies as marked in the figure,  $\omega_{sr}$  for the reference chirp and  $\omega_{sj}$  for the  $j$ th control chirp ( $j = 1, 2, \dots$ ). Each pair of the reference and the control chirps program a spatial-spectral grating in the medium. The period of the spectral grating is determined by the chirp rate and the frequency offset between the control and the reference as,  $(\omega_{sr} - \omega_{sj})/\beta$  for the  $j$ th control chirp. A brief pulse along  $\vec{k}_-$  direction probes the gratings results in multiple echoes along  $\vec{k}_+$ , each from a different grating with the corresponding delay,  $\tau_j = \beta/(\omega_{sr} - \omega_{sj})$  created by a control chirp and the reference. These generated echoes can be used as temporal bits to compose any arbitrary waveform provided the delays, the amplitudes,

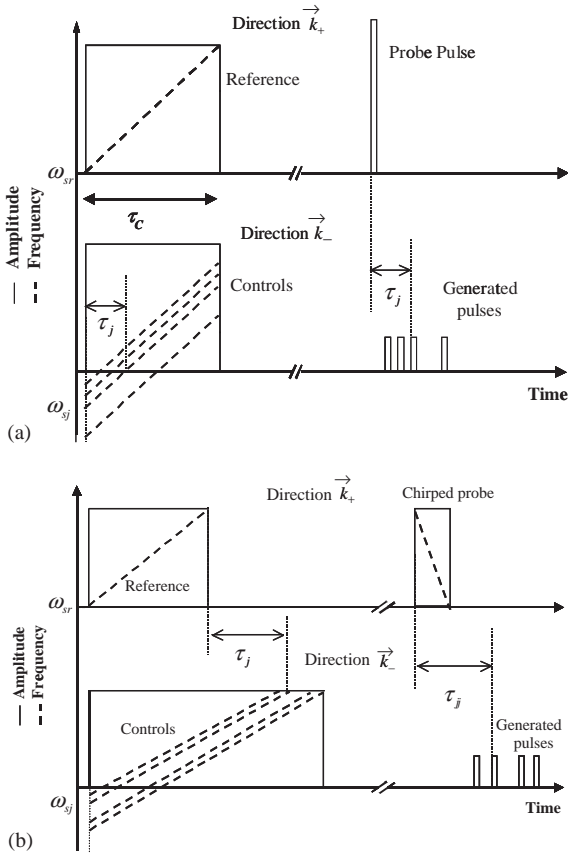


Fig. 1. The photon echo process for pulse shaping and AWG. The spectral gratings are programmed by multiple frequency chirped pulses and probed by either a brief pulse (a) or a frequency chirped pulse (b). The reference and the probe pulses chirp propagate along directions  $\vec{k}_+$  while the control pulses and the generated echo sequence along  $\vec{k}_-$ .

and the phases of each of the echo pulse can be controlled individually. It has been demonstrated that these indeed can be controlled by the amplitudes and the phases of the control pulses together with the frequency offsets from the reference chirp [5]. In the linear programming regime the echo's amplitude is proportional to the amplitude of the control chirp. The echo's phase is more complicated since the reference and the control chirps impart a phase shift to the echo depending on the chirp rate and the starting frequencies. This phase shift usually needs to be compensated. Fig. 1(b) shows a scheme where the

control pulses are chirped at a different rate from the reference and the probe is a linear chirp as well. In this case the echoes' rephrasing condition and the phase compensation are more complicated compared to the scheme in Fig. 1(a). In the next section we derive the analytic solution for the two schemes in Fig. 1 for ideal chirps.

### 3.1. Theoretical analysis on the chirp rates and phase compensation

First we consider the grating programmed by a pair of the reference and the control chirps whose field can be written in a form as

$$\varepsilon(t) = E_0 e^{i[(\omega_0 + \omega_s)t + \frac{1}{2}\beta t^2] + i\phi} = E_c(t) e^{i\omega_0 t} \quad (12)$$

with  $E_c(t) = E_0 e^{i\omega_s t + i\frac{1}{2}\beta t^2 + i\phi}$ .  $\omega_0$  is the arbitrary stationary frequency discussed in the previous section, usually set to the center frequency of the probe pulse. The spectrum of the chirp is given by the Fourier transform as

$$\begin{aligned} \tilde{E}_c(\omega) &= \int E_c(t) e^{-i\omega t} dt \\ &= A' e^{-i\frac{(\omega_s - \omega)^2}{2\beta}} e^{i\frac{\pi}{4} \text{sign}(\beta) + i\phi}, \end{aligned} \quad (13)$$

where the spectrum amplitude has the form of  $A' = E_0 \sqrt{2\pi/|\beta|}$  and function  $\text{sign}(\beta)$  returns the sign of  $\beta$ . A positive chirp rate corresponds to a upward chirp from low frequency to high frequency. Expression (10) represents an ideal frequency chirped pulse, which has uniform amplitude in both temporal and spectral domain. The linear frequency chirp in time results in a spectral phase changing quadratically with the frequency. It is a good approximation for the chirped field with time bandwidth product (TBP)  $\gg 1$ . Even for small TBP, the amplitude of the spectrum is no longer uniform while the spectral phase term is still the same.

The spectral grating generated by the two frequency chirped pulses (the reference and one control) in linear programming regime can be expressed as,

$$\begin{aligned} \tilde{G}(\omega) &= \tilde{E}_r^*(\omega) \tilde{E}_j(\omega) = A'_r A'_j e^{-i\frac{(\omega_{sj} - \omega)^2}{2\beta_j} + i\frac{(\omega_{sr} - \omega)^2}{2\beta_r}} \\ &\quad \times e^{i\phi_j - i\phi_r + i\frac{\pi}{4}[\text{sign}(\beta_j) - \text{sign}(\beta_r)]}, \end{aligned} \quad (14)$$

where subscript  $r$  is for reference pulse and  $j$  is for  $j$ th control pulse. Probing the spectral grating with a pulse with the spectrum denoted as  $\tilde{E}_p(\omega)$ , the echo's spectrum takes the shape of  $\tilde{G}(\omega)\tilde{E}_p(\omega)$ . The probe spectrum can be either chirp or brief pulse, which results in the echo spectrum as,

$$\tilde{E}_{\text{echo}}(\omega) = \begin{cases} A e^{-i\frac{\omega^2}{2}\left(\frac{1}{\beta_j}-\frac{1}{\beta_r}\right)} e^{-i\omega\left(t_p+\tau_{jr}-\frac{\omega_{sj}}{\beta_j}+\frac{\omega_{sr}}{\beta_r}\right)} e^{-i\frac{\omega_{sj}^2}{2\beta_j}+i\frac{\omega_{sr}^2}{2\beta_r}+i\varphi_j-i\varphi_r} \\ \quad \times e^{i\frac{\pi}{4}[\text{sign}(\beta_j)-\text{sign}(\beta_r)]} & \text{for brief probe} \\ A e^{-i\frac{\omega^2}{2}\left(\frac{1}{\beta_p}+\frac{1}{\beta_j}-\frac{1}{\beta_r}\right)} e^{-i\omega\left(t_p+\tau_{jr}-\frac{\omega_{sp}}{\beta_p}-\frac{\omega_{sj}}{\beta_j}+\frac{\omega_{sr}}{\beta_r}\right)} \\ \quad \times e^{-i\frac{\omega_{sp}^2}{2\beta_p}-i\frac{\omega_{sj}^2}{2\beta_j}+i\frac{\omega_{sr}^2}{2\beta_r}+i\varphi_p+i\varphi_j-i\varphi_r} \\ \quad \times e^{i\frac{\pi}{4}[\text{sign}(\beta_p)+\text{sign}(\beta_j)-\text{sign}(\beta_r)]} & \text{for chirped probe,} \end{cases} \quad (15)$$

where the amplitude  $A$  is determined by the amplitudes of all three pulses and the chirp rates.  $\omega_{sp}$  denotes the starting frequency of the probe chirp. For the purpose of pulse shaping and AWG, the coherence from all frequencies should be rephased at the same instant as a brief echo pulse. This implies that the phase of the echo should not be a quadratic function of the frequency for both cases with brief and chirp probe. This set the rules for the chirp rate of the rephrasing condition as

$$\begin{aligned} \beta_r &= \beta_j & \text{for brief probe,} \\ \frac{1}{\beta_p} + \frac{1}{\beta_j} - \frac{1}{\beta_r} &= 0 & \text{for chirped probe.} \end{aligned} \quad (16)$$

The second phase term in the above Eq. (12) determines the time delay of the rephased echo compared with the starting time of the probe pulse,

$$\tau_j = \begin{cases} \frac{\omega_{sr} - \omega_{sj}}{\beta_r} & \text{for brief probe,} \\ \frac{\omega_{sp}}{\beta_p} - \frac{\omega_{sj}}{\beta_j} + \frac{\omega_{sr}}{\beta_r} & \text{for chirped probe.} \end{cases} \quad (17)$$

From the third phase term in expression (12) we can see that the echo's phase can be controlled by setting a designed phase factor into the control pulse. However, for the purpose of control the phase of each individual echo pulse, all the echoes from different combinations of reference, control

and probe pulses should have the same phase standard. This means the echo's phase should not depend on any parameters of the input pulses other than the designed control phase. To ensure this, we add a phase compensation to each chirp by setting the arbitrary phase terms for the reference and the probe as,  $\varphi = \omega_s^2/2\beta$  and the phase term for the control pulse as,  $\varphi_j = \omega_{sj}^2/2\beta_j + \varphi_{cj}$ , where  $\varphi_{cj}$  represents the control phase for the  $j$ th echo to compose the desired waveform. The phase compensation guarantees the echoes from any combination of reference, control, and probe chirps have the same phase when the control phase is set to zero. In the cases presented in Fig. 1, to generate an arbitrary waveform out of either a brief or a chirped pulse, we only need to work out the amplitudes, the phases, the chirp rates, and the frequency offsets needed for the reference and the control pulses according to the analysis presented above. Furthermore, the conditions of echo rephasing (13) and (14) and the phase compensation do not set any limit on the numbers of the pulses in the reference, the control, and the probe categories. The analytic results can be used to design even more complicated pulse sequence.

### 3.2. Numerical simulation and experimental results

The Maxwell–Bloch model discussed in Section 2 allows the arbitrary phase modulation in angled beam setting. In the following simulations for pulse shaping and AWG, the general phase term of a chirp has two time-dependent components:  $\omega_s t + \frac{1}{2}\beta t^2$ , a static phase compensation  $\omega_s^2/2\beta$ , and a control phase  $\varphi_{cj}$  for the control chirp. The time-dependent phase of a chirped pulse results in the oscillations of the field components in the rotating frame and the oscillation frequency is time dependent. In the numerical solution of the Maxwell–Bloch equations, the temporal resolution should be high enough to distinguish the finest temporal structure. Usually, this requires more calculation steps on the time grid than the case for brief pulse while the spectral and spatial resolutions are the same for both cases. The number of calculation steps should increase with both the chirp rate and the chirp offset. Fig. 2 shows the oscillation of the field in rotating frame due to the

time-dependent phase for a frequency chirped field with 20 MHz bandwidth and 5  $\mu$ s chirp time. The time resolution is 3 ns per point, which gives 35 steps for a cycle of the highest oscillation frequency in the two ends of the chirped field.

In Fig. 3 an 11 bits Barker code series, in the modulation format at 10 Mbit/s, was generated with the setting described in Fig. 1(a). The reference pulse (as shown in Fig. 2) and 11 control pulses are 5  $\mu$ s-long, linear frequency chirped over 20 MHz. The relative frequency offset for the  $j$ th control from the reference chirp was  $0.4*j$  MHz.

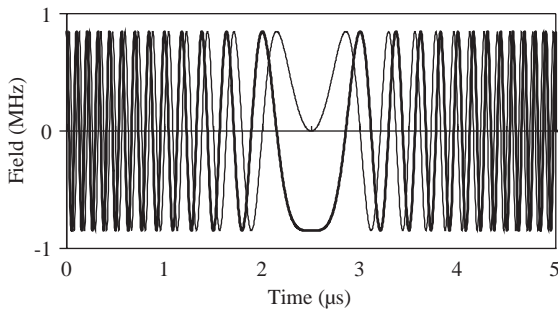


Fig. 2. The frequency chirped field in a rotating frame. The thick line is the in-phase field component and the thin line is the quadrature component. The field is a frequency chirped pulse with 20 MHz chirp bandwidth, 5  $\mu$ s chirp time, and zero frequency offset. 35 steps are in a cycle of the highest oscillation frequency.

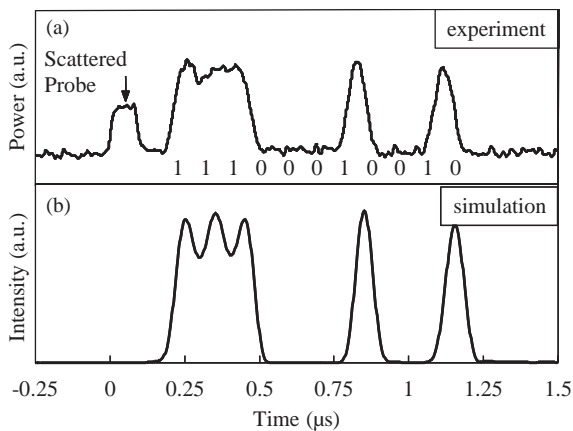


Fig. 3. An 11-bit Barker code (11100010010) generated as a photon echo sequence with the scheme described in Fig. 1(a). The echo bandwidth is 10 MHz and the code bit rate is 10 Mbit/s. (a) Experimental data and (b) the simulation result.

The chirp rate and the frequency offset define the bit rate of the generated code, which is 10 MHz in this case. The phase compensation was also added to each control chirp. The probe is a 100 ns brief pulse, which determines the pulse width of each echo since the programmed spectral gratings are broader than the probe pulse spectrum. Fig. 3(a) shows the power of the echo sequence representing the 11 bits barker code (11100010010) from an experiment [5] and Fig. 3(b) gives the simulation result as the intensity of the echo field. The code is well represented by the echo sequence in both the experiment and the simulation. In Fig. 4, the same code was generated in the binary phase shift format (111-1-1-11-1-11-1), which was produced with the same parameters for the input pulses except for a  $\pi$  phase shift added to the control pulses for the echoes representing the  $-1$ s. The experimental result is plotted in Fig. 4(a) as the echo power and the simulation results of the echo sequence as the intensity is plotted in Fig. 4(b) and the amplitude in Fig. 4(c). The nulls on the power and the intensity plots correspond to the phase flip

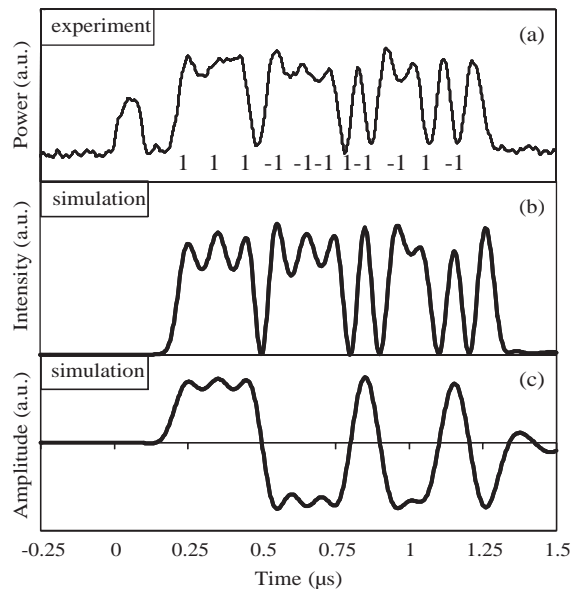


Fig. 4. An 11-bit Barker code (111-1-1-11-1-11-1) generated as a photon echo sequence with the scheme described in Fig. 1(a). The echo bandwidth is 10 MHz and the code bit rate is 10 Mbit/s. (a) Experimental data and (b) the simulation result.

representing the bi-phase code. The simulations in Figs. 3 and 4 show good agreement with the experiments.

Fig. 5 presents the simulations for the scheme plotted in Fig. 1(b) where the reference, the control, and the probe pulses are linear chirped at different chirp rates that meet the rephasing requirement (13). In this case the same 11 bit amplitude modulated barker code is generated at high bit rates with broadband chirps. The bandwidths for all chirps are 20 GHz. The reference is a 6 ns upward chirp and the probe is a 1 ns down chirp. The controls are 7 ns up chirps. In Fig. 5(a) the frequency offset was set to  $300*j$  MHz for the  $j$ th control. This results in the code sequence with 9.5 Gbit/s. The bandwidth of each echo pulse is 20 GHz determined by the spectral overlap range of all chirps. In this case we have a series of well-distinguished return-to-zero (RZ) code. In Fig. 5(b) the frequency offset between the adjacent control pulses was decreased to 150 MHz so that the bit rate was doubled to 19 Gbit/s for the same echo bandwidth. The code is still well represented in a non-return-to-zero (NRZ) form. To keep the code in RZ format, the echo bandwidth needs to

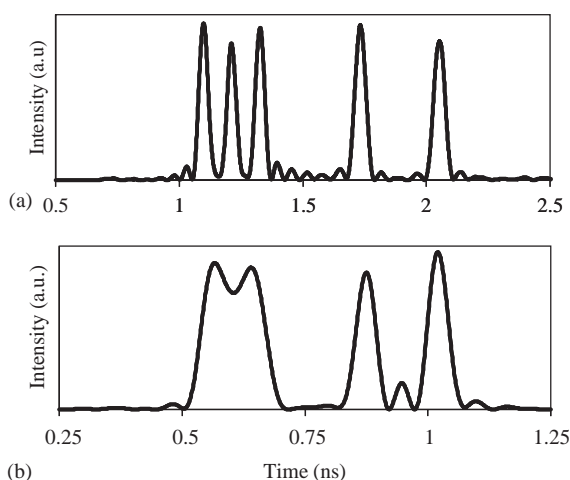


Fig. 5. Simulations for the high band code generation of an 11-bit Barker code in binary amplitude modulation format (11100010010) using the scheme described in Fig. 1(b). (a) RZ code produced at 9.5 Gbit/s with echo bandwidth of 20 GHz. (b) NRZ code produced with 19 Gbit/s with echo bandwidth of 20 GHz.

be at least twice broader than that required for the NRZ format at the same bit rate. This in turn requires higher chirp bandwidth.

#### 4. Conclusion

We have derived a theoretical model based on Maxwell–Bloch equations for OCT processes of angled beam configuration with arbitrary phase modulation. A numerical simulation tool with running time practical for studying complex features has been developed. Using this numerical tool, the OCT processes of angled beam geometry with the pulses of frequency offsets and chirps and the phase shifts can be simulated. The model can be extended to include the laser noise. The OCT pulse shaper and AWG have been analyzed as an important example of angled-beam with complex frequency and phase modulations. The rephasing condition and the phase compensation required for two possible programming and probe schemes has been derived analytically for ideal chirp condition and verified under realistic conditions in experiments and with simulations. The simulation and experimental results for code generating at low bandwidth agree with each other very well. We also simulated high bandwidth code generating, which provides useful guideline for high bandwidth experiments.

#### Acknowledgements

The authors would like to acknowledge the support from a DARPA Grant (MDA972-03-1-0002) and a AFOSR DEPSCoR Grant (F49620-02-1-0275).

#### References

- [1] T.W. Mossberg, *Opt. Lett.* 7 (1982) 77.
- [2] W.R. Babbitt, J.A. Bell, *Appl. Opt.* 33 (1994) 1538.
- [3] W.R. Babbitt, T.W. Mossberg, *Opt. Lett.* 20 (1995) 910.
- [4] K.D. Merkel, W.R. Babbitt, *Opt. Lett.* 21 (1996) 1102.

- [5] Zeb W. Barber, Mingzhen Tian, Randy R. Reibel, W. Randall Babbitt, *Opt. Express* 10 (2002) 1145.
- [6] T. Chaneliere, S. Fraigne, J.-P. Galaup, M. Joffre, J.-L. Le Gouet, J.-P. Likforman, D. Ricard, *Eur. Phys. J. AP* 20 (2002) 205.
- [7] H. Schwoerer, D. Erni, A. Rebane, *J. Opt. Soc. Am. B* 12 (1995) 1083.
- [8] A.M. Weiner, *Prog. Quant. Electron.* 19 (1995) 161.
- [9] R.W. Olson, H.W.H. Lee, F.G. Patterson, M.D. Fayer, *J. Chem. Phys.* 76 (1982) 31.
- [10] M. Azadeh, C. Sjaarda Cornish, W.R. Babbitt, L. Tsang, *Phys. Rev. A* 57 (1998) 4662.
- [11] C. Greiner, B. Boggs, T. Loftus, T. Wang, T.W. Mossberg, *Phys. Rev. A* 60 (1999) R2657.
- [12] T. Wang, C. Greiner, J.R. Bochinski, T.W. Mossberg, *Phys. Rev. A* 60 (1999) R757.
- [13] T. Wang, C. Greiner, T.W. Mossberg, *Opt. Commun.* 153 (1998) 309.
- [14] T. Chang, M. Tian, W.R. Babbitt, in these Proceedings (HBSM 2003), *J. Lumin* 107 (2004), previous article.